

Practice and Technology, 14(2), pp. 297-310. <https://doi.org/10.2166/wpt.2019.014> and is available at <https://iwaponline.com/wpt/article/14/2/297/65983/Nanofibers-for-textile-waste-water-management>

1 **Nanofibers for textile waste water management**

2 Joginder singh Paneysar<sup>a</sup>, Snehal Sawant<sup>a</sup>, Meng Hei Ip<sup>c</sup>, Sukhwinder kaur Bhullar<sup>b,\*</sup>, †,  
3 Stephen Barton<sup>c</sup>, Premlata Ambre<sup>a†</sup>, Evans Coutinho<sup>a</sup>

4

5 <sup>a</sup>Department of Pharmaceutical Chemistry, Bombay College of Pharmacy, Mumbai 400 098,  
6 India.

7 <sup>b</sup>Department of Mechanical Engineering, Bursa Technical University, Bursa 16190, Turkey.

8 <sup>c</sup>School of Life Sciences, Pharmacy and Chemistry, Kingston University, Kingston-upon-  
9 Thames, KT1 2EE, UK

10

11 \* Current address: Sukhwinder K Bhullar

12 St. Boniface Hospital, Albrechtsen Research Centre, Winnipeg, MB, Canada

13

14 †Authors for correspondence

15 Tel: (022) 26670871 Extn. 241

16 E-mail: [premlata.ambre@bcp.edu.in](mailto:premlata.ambre@bcp.edu.in)

17 E-mail: [sbhullar@sbrca.ca](mailto:sbhullar@sbrca.ca)

18

19 **Abstract**

20 Currently, textile wastewater management focusses on dye removal efficiency and operating costs. Dual  
21 responsive polymers are choice materials because they can extract diverse organic compounds from  
22 water at their phase transition point. They are copolymers of the acrylamide class, and have been fully  
23 characterized by FT-IR, <sup>1</sup>H-NMR, DSC, GPC and surface area analysis. Of the five dual responsive  
24 polymers, the copolymer of NIPAAM and DMAEMA (CoP-1) offers the best extraction of acidic and  
25 basic dyes from wastewater. All copolymers investigated can achieve better than 90% dye removal  
26 when used at 4 mg/ml concentration. This dye-scavenging efficiency increases to almost 99% at 3  
27 mg/ml, on conversion of the copolymers to nanofibers in 300 to 500 nm size. Langmuir and Freundlich  
28 isotherms were constructed to study the mechanism of dye adsorption. The nanofibers have been shown  
29 to be reusable for removal of dyes from water, suggesting that such systems may add benefit to current  
30 dye removal methods from textile industry wastewater.

31 **Keywords**

32 Adsorption isotherm, dual responsive polymers, smart nanofibers, textile dyes, textile water  
33 management

34

## 35 **Introduction**

36 Water shortages and stringent regulatory strictures in recent years have encouraged the development of  
37 novel systems for water reuse. Providing potable water at a rate to match increase in population with  
38 decrease in water quality, available resources and climate change is a great challenge (Robinson *et al.*,  
39 2001). The textile industry is a prime culprit in water pollution, posing risk to human and aquatic life.  
40 The industry produces around 80 million tonnes of fibers per year (mt/a) and total dye consumption for  
41 these fibers exceeds 1 mt/a. Textile dye concentrations are usually between 10 and 200 mg/L, and about  
42 10 to 15% of the dye is lost in the process (Liang *et al.*, 2014). Further processing, including washing,  
43 releases more dye, which is drained as effluent. These dyes increase the turbidity of water, and make it  
44 look and smell bad, additionally inhibiting the penetration of sunlight necessary for photosynthesis.  
45 Dissolved oxygen is essential for life in water and its depletion is the most serious effect of textile waste  
46 discharge, which also hinders natural purification processes.

47 Stringent laws have been proposed that limit the amounts and kinds of waste that can be released as  
48 effluent. The extensive release of textile dyes with adverse effects on the environment and public health,  
49 means that serious efforts are required to reduce pollution. This can be achieved using efficient effluent  
50 treatment systems at textile industry sites. Various methods have been devised for treatment of dye  
51 wastewaters which can be broadly classified as physical, chemical and/or biological, depending on the  
52 application. Physical methods include adsorption, membrane filtration, irradiation, coagulation, reverse  
53 osmosis, ultra-filtration and nanofiltration. Of all these technologies, adsorption is the simplest and is  
54 effective as it offers high removal efficiency for a wide spectrum of dye-types (Elmoubarki *et al.*, 2015).  
55 No additional materials are needed to operate these processes, thereby offering high efficiency, and  
56 helping to preserve available water resources by both increased efficiency and ease of operation.

57 Nanotechnology is used in adsorption in various forms like nanoparticles, nanotubes and nanofibers,  
58 and has the potential to remove metal ions, dyes, and various organic and inorganic species. In  
59 particular, polymeric nanofibers have become popular in the past few years for removal of contaminants  
60 from water. The non-woven material produced by electrospinning has several attractive features  
61 including diameter below 500 nm, large surface area, high porosity, high gas permeability and small

62 pore size. Swaminathan et al (2015) report on use of an electrospun nanofibrous composite mat prepared  
63 from polyacrylonitrile (PAN) yarn waste and graphene oxide for removal of methylene blue from water.  
64 Electrospun polyvinylalcohol/titanium oxide (PVA)/TiO<sub>2</sub> composite membranes followed by  
65 photocatalysis have also been reported to remove methylene blue from water (Ismaya *et al.*, 2017).  
66 Chen et al (2016) report dye removal using cellulose-based graphene oxide fibres, demonstrating the  
67 extensive capability of polymers.

68 Dual responsive polymers are a class of materials that exhibit different properties at different  
69 temperature and pH ranges. Dual responsive polymeric microgel-based assemblies have already  
70 established efficiency for removal of organic dyes from water (Parasuraman and Serpe, 2011). With  
71 respect to temperature response, these polymers are soluble in water at room temperature but precipitate  
72 at higher temperatures. Likewise, pH responsive polymers are completely soluble in water over a certain  
73 pH range but precipitate just outside it. The transition point from soluble to insoluble, triggered by  
74 temperature or pH, is termed the cloud point (CP) and defined as the first appearance of turbidity for a  
75 clear polymeric solution. Lower critical solution temperature (LCST) is used in relation to temperature  
76 responsive polymers and is the point above which the polymer chains start orienting themselves in such  
77 a manner that hydrogen bonding efficiency is reduced, and the chains become hydrophobic. This  
78 hydrophobic state is responsible for the adsorption of most organic contaminants from water (Paneysar  
79 *et al.*, 2017). The temperature responsive polymers include the acrylamide class – e.g., poly(N-  
80 isopropylacrylamide) [PNIPAAm], poly(N,N-diethylacrylamide) [PNNDEA], poly(N-  
81 vinylcaprolactum) [PNVCL], poly(N-vinyl isobutyramide) [PNVIB], etc – whereas the pH responsive  
82 polymers include polyvinylpyrrolidone [PVP], polyacrylic acid [PAA], polymethacrylic acid [PMA],  
83 polyethylacrylic acid [PEA], poly propylacrylic acid [PPA], etc. The monomers from the two  
84 categories, when copolymerized, yield polymers that respond to both temperature and pH at the phase  
85 transition point (Liang *et al.*, 2015), and are classified as dual responsive polymers. They include poly  
86 dimethylaminoethyl methacrylate (PDMAEMA) and poly diethylaminoethyl methacrylate  
87 (PDEAEMA), both available commercially. Dual responsive polymers have reportedly been used for  
88 peptide (Aguilar *et al.*, 2007), DNA (Hinrichs *et al.*, 1999), transdermal (Samah and Heard, 2013), and

89 drug delivery systems (Zheng *et al.*, 2017) for anticancer therapy (Zhu *et al.*, 2010), as well as dye  
90 removal from wastewater (Marques *et al.*, 2015).

91 This study focuses on the development of dual responsive polymers and evaluation of their application  
92 in textile wastewater treatment. Water discharged by the textile industry is usually at higher than  
93 ambient temperature and with varied pH, so the properties of dual responsive polymers could be  
94 appropriate under these conditions. These polymers and their nano-fabricated products – nanofibers –  
95 were evaluated in the study. Since textile wastewater has dyes as the primary component, the aim was  
96 their removal with maximum efficiency.

## 97 **Materials and Methods**

### 98 **Materials**

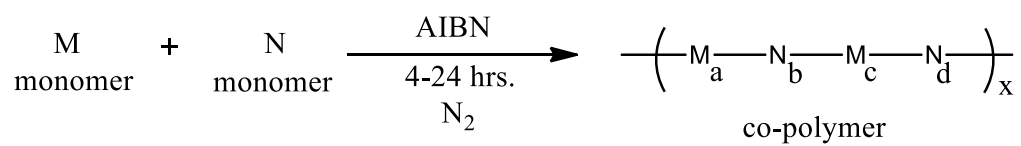
99 The monomer N-isopropylacrylamide (NIPAAM) was obtained as a gift sample from SLN Pharma  
100 chem (Mumbai, India), and dimethylaminoethyl methacrylate (DMAEMA) was a gift sample from Ess  
101 Emm chemicals (Mumbai, India), diethylacrylamide (DEA) was procured from TCI chemicals  
102 (Chennai, India) and vinylpyrrolidone (VP) from Sigma-Aldrich (Mumbai, India). The free radical  
103 initiator azobisisobutyronitrile (AIBN) was purchased from Spectrochem Pvt. Ltd (Mumbai, India) and  
104 dialysis membrane from HiMedia (Mumbai, India).

### 105 **Methods**

#### 106 **Synthesis of smart dual responsive polymers**

107 The monomers were combined and dissolved in 5 ml ethanol in different weights and ratios – see Table  
108 1. The initiator (AIBN) was added under a nitrogen atmosphere and the reaction was carried out at 70  
109 °C to initiate polymerization. The ethanol in the medium was removed under vacuum using a rotary  
110 evaporator, after which the viscous solution was poured into hexane and the precipitate dissolved in  
111 ethyl acetate. This was repeated 2 or 3 times to remove starting materials and reactants, and the crude  
112 copolymer was dried under vacuum. The copolymer was purified by dialysis against distilled water for  
113 3 days in a membrane with a molecular weight cut-off of 12,000 to 14,000 Da. After dialysis the

114 solutions were lyophilized, giving free-flowing powders. Table 1 gives details of the monomer and  
115 agent ratios used for copolymerization, and Figure 1 shows the general copolymerization scheme.



116 where, a, b, c, d, x = 1, 2, 3.....n

117 **Figure 1. General copolymerization scheme**

118

Code	Copolymer	Monomers				Initiator (AIBN)	Solvent (Ethanol)	Time (Hrs.)	LCST (°C)	Cloud point (pH)
		NIPAAM	DEA	VP	DMAEMA					
CoP-1	NIPAAM- DMAEMA (14:1)	1.1 Gm (10 mmol)	-	-	118 µl (0.7 mmol)	10 mg	5 ml	24	37	10.0
CoP-2	DEA-DMAEMA (1:14)	-	700 µl (5.76 mmol)	-	60 µl (0.41 mmol)	10 mg	5 ml	10	28	9.5
CoP-3	NIPAAM-VP (1:1.5)	0.425 gm (3.86 mmol)	-	0.55 ml (5.1 mmol)	-	10 mg	5 ml	09	30	12.0
CoP-4	DEA-VP (10:1)	-	700 µl (5.76 mmol)	60 µl (0.56 mmol)	-	10 mg	5 ml	24	45	10.5
CoP-5	DMAEMA-VP (5:1)	-	-	770 µl (6.55 mmol)	210 µl (1.27 mmol)	10 mg	5 ml	4	50	9.0

**Table 1. Quantities of reactants and time taken for copolymerization, and respective polymer cloud points**



## 120 **Electrospinning**

121 CoP-1 (0.6 gm); CoP-2 (0.15 gm); CoP-4 (0.7 gm) and undiluted polycaprolactone (PCL) (0.8 gm)  
122 were individually dissolved in chloroform to obtain a 10% w/v polymer solution for fabrication of  
123 nanofibers NF-1, NF- 2, NF- 4 and PCL respectively. Electrospinning was carried out at 30 kV and  
124 0.25 ml/min flow rate, using an Inovenso Nanospinner<sup>24</sup>. Nanofibers were collected on a drum covered  
125 with aluminium foil rotating at 100 rpm. The collector/needle distance was 10 cm and 10 ml of solution  
126 was used completely for each sample to spin the same amount of fibre each time. The nanofibers were  
127 dried in a fume hood for 24 hours at room temperature.

## 128 **Determination of CP/LCST of the copolymer under the influence of temperature and pH**

129 LCST was determined by the cloud point method – visual examination – by increasing the temperature  
130 linearly of a 2.5% solution of copolymer from 20 to 40°C. The temperature at which the solution turned  
131 turbid was noted as the CP (the temperature at which the polymer precipitated), and expressed as the  
132 LCST. The CP was confirmed using a Mettler (Toledo) DSC 822e unit. Similarly, the pH of the polymer  
133 solutions was varied from 2 to 13 and the point of first appearance of turbidity was noted.

## 134 **FT-IR analysis**

135 Potassium bromide (KBr) discs with the copolymers were prepared using an electrically operated  
136 Techno Search Instruments KBr press model HP-15 (Mumbai, India). IR spectra were recorded on a  
137 Jasco FTIR-5300 Fourier transform spectrophotometer with a resolution of 4 cm<sup>-1</sup>.

## 138 **<sup>1</sup>H-NMR characterization**

139 NMR spectra of the copolymers were recorded using a Brüker Avance III 800 MHz FT-NMR  
140 spectrometer. The NMR samples were each made in solution comprising 0.9 ml H<sub>2</sub>O and 0.1 ml D<sub>2</sub>O.

## 141 **Molecular weight determination**

### 142 **Gel permeation chromatography (GPC)**

143 GPC was performed with a Varian Pro Star 210 solvent delivery module and a Phenomonex Yarra 3u  
144 SEC-4000 aqueous GPC column (column size 300 x 7.8 mm). Data collection was driven by Galaxie

145 Chromatography Software; 100 mM Na<sub>2</sub>HPO<sub>4</sub> buffer (pH 6.8) was used as the mobile phase at a  
146 constant flow rate of 1 ml/min. All polymer samples were detected by UV at 280 nm. GPC standards  
147 were used to calibrate the instrument prior to sample analysis. Twenty µl of the calibration standard  
148 solution (protein mixture and uridine) was injected in each case and the analysis run for 20 minutes.

#### 149 **Surface area determination**

150 Brunauer-Emmett-Teller (BET) surface area analysis and Barrett-Joyner-Halenda (BJH) pore size and  
151 volume analysis were performed on a Belsorp Mini II (Metrohm). Nitrogen adsorption and desorption  
152 by the polymer were studied. The measuring range of the instrument for surface area was 0.01 m<sup>2</sup>/g and  
153 pore size 0.35 to 200 nm. A weighed sample was loaded into a glass tube and, as pre-treatment, was  
154 degassed for 3 hours at 110 °C and 10<sup>-2</sup> kPa pressure. The sample was then rechecked to obtain the  
155 actual weight and the sample cell (glass tube) loaded into the instrument for analysis.

#### 156 **Nanofiber characterization**

157 The surface morphology of the nanofibers was studied by scanning electron microscopy (SEM). The  
158 average nanofiber diameter was measured from images captured with a ZEISS EVO 40 microscope and  
159 sputter-coating was done with BAL-TEC SCD 005. The samples were prepared on a base coating of  
160 gold-palladium (60% : 40%) to make them appropriate for electron sample interaction. The sample was  
161 coated for 100 to 200 seconds to a thickness between 5 and 30 nm. After coating, the samples were kept  
162 in the SEM chamber and the system was subjected to high vacuum while imaging.

163

164 **Evaluation and optimization of adsorption potential**

165 Dyes are released daily as effluents by the textile industry, and may be classified as acidic, basic, direct,  
166 mordant, vat, reactive, disperse, azo and/or sulphur dyes. Methylene blue and crystal violet were  
167 selected as representative basic dyes, whereas Congo red, methyl orange, and indigo carmine were  
168 selected to represent acidic dye species for the study. The proportional dye removal by the co-polymers  
169 was evaluated by UV-visible spectroscopy.

170 A fixed concentration of each dye with absorbance within the linear range of the Beer-Lambert law was  
171 selected, and the solutions treated with the co-polymers and nanofibers. The conditions for adsorption  
172 were optimised by varying the copolymer concentration and the contact time above the respective CPs.  
173 Two copolymer concentrations, 1 and 4 mg/ml, were added to the dye solution and heated above the  
174 CP for various times. The solutions were then filtered, the precipitate removed and the absorbance of  
175 the final solution measured by UV. The proportional dye removal was calculated using Equation (1):

$$176 \quad \text{proportional dye removal} = \frac{C_o - C_e}{C_o} \times 100$$

177 (1)

178 where,  $C_o$ : dye concentration before treatment, and  $C_e$ : dye concentration after equilibrium and  
179 treatment

180 All the proportional removal or adsorption analysis studies were performed in triplicate.

181 **Adsorption parameter optimization**

182 The copolymers are highly soluble in water and precipitate only above the cloud point (CP).  
183 Precipitation is caused by transformation of the copolymer into hydrophobic coiled chains that are  
184 responsible for absorption of the dye. To determine the polymers' maximum adsorption ability initially,  
185 a low concentration (1 mg/ml) of copolymer was added to a solution containing a fixed concentration  
186 of dye (methylene blue – 3mg/L). The solution temperature and pH were increased steadily, and then  
187 kept constant above the individual polymers' CPs for a range of times. The proportional adsorption was  
188 calculated for various times to determine the maximum dye adsorption. In a second study, the polymer  
189 concentration was kept at 4 mg/ml and the adsorption time for equilibrium determined.

190 Since, the adsorption of impurities depends largely on the polymer's specific surface area, it was  
191 decided to test the polymers' power when fabricated as nanofibers. Different weights of nanofibers were  
192 used for removal of dye from water above the LCST and pH responsive CP . The difference between  
193 the UV-visible absorbance of the dye solution before (inlet) and after (outlet) passing through the  
194 nanofibers was calculated to determine the amount of dye adsorbed. Since all nanofibers were blended  
195 with PCL for fabrication, blank PCL nanofibers were also evaluated for removal of dye from water.

#### 196 **Optimization of adsorption potential using nanofibers**

197 Between 5 and 50 mg of nanofibers were taken, in 5 mg intervals, and tested for dye removal.  
198 Proportional removal of dye was at a maximum with 30 mg of nanofiber (3 mg/ml) for 10 ml methylene  
199 blue solution(3 mg/L), and this concentration was then fixed with the optimised contact time at  
200 respective temperature and pH to evaluate removal by nanofibers. Similarly, adsorption by PCL  
201 nanofibers was also studied at the same concentration and it was found that these 'blank' nanofibers  
202 could also adsorb dyes from water.

#### 203 **Determination of particle size of copolymer at CP**

204 To measure the particle size at LCST and CP, copolymer CoP-1 was dissolved in water to prepare two  
205 solutions each of 2.5% concentration. The temperature and pH of the solutions were increased slowly,  
206 and the particle size beyond the CP was measured with a Malvern Zetasizer Nano ZS.

#### 207 **Adsorption isotherm determination (Akl and Abou-Elanwar, 2015)**

208 Sorption isotherm studies were used to determine and explain the relationship between  $C_{eq}$ , the  
209 equilibrium concentration of the adsorbate (the copolymers), and the amount adsorbed at the surface.  
210 The Langmuir and Freundlich isotherm models were used to analyse the copolymers above their CPs  
211 at the optimised temperatures, pHs and contact times.

#### 212 **Langmuir adsorption isotherm**

213 The Langmuir model exhibits a linear relationship for the amount of dye adsorbed per unit mass of  
214 adsorbent copolymer. It is distinguished by three factors – adsorption, desorption and kinetic rates –  
215 combined with the total number of free sites available on the surface. The collective surface  
216 concentration of dye is denoted by  $q$ .

217 Equation (2) is the linear form of the Langmuir equation:

$$218 \quad \frac{C_e}{q_e} = \frac{1}{q_m K_L} + \frac{C_e}{q_m} \quad (2)$$

219 where,  $q_e$  (mg/g) is the amount of dye adsorbed per unit mass of copolymer (sorberent),  $C_e$  (mg/l) the final  
220 concentration of unadsorbed dye in solution,  $q_m$  (mg/g) the monolayer adsorption capacity and  $K_L$  (l/mg)  
221 the Langmuir equilibrium constant.

222  $q_e$  is expressed as,

$$223 \quad q_e = \frac{(C_i - C_f)V}{mass} \quad (3)$$

224 where,  $C_i$  is the initial concentration,  $C_f$  the final concentration, and  $V$  the volume of dye solution. The  
225 volume of dye and mass of polymer remain constant for a given set of analyses.

226 A graph of  $\frac{C_e}{q_e}$  against  $C_e$  gives the Langmuir isotherm

### 227 **Freundlich adsorption isotherm**

228 This isotherm was developed using the assumption that the adsorbent has a heterogeneous surface with  
229 numerous adsorption sites.

230 The linear form of the Freundlich equation is (4):

$$231 \quad q_e = K_f C_e^{1/n} \quad (4)$$

232 where  $n$  is the Freundlich exponent and  $K_f$  the Freundlich constant, which measures heterogeneity; the  
233 higher  $K_f$ , the more heterogeneous the adsorbent. To determine the Freundlich isotherm a plot of  $\log q_e$   
234 against  $\log C_e$  gives a slope equal to  $1/n$  and an intercept at  $\log K_f$ . The slope  $1/n$  represents a collective  
235 value of the relative magnitude of adsorption intensity for a certain sorption process.

$$236 \quad \log q_e = \log K_f + \frac{1}{n} \log C_e \quad (5)$$

237 To determine the applicability and suitability of a specific isotherm model to the experimental data,  
238 regression coefficient ( $R^2$ ) values were calculated from the plot of  $\log q_e$  v/s  $\log k_f$ . Comparison of the  
239 two models is based on the value of  $R^2$ . The Langmuir constants are obtained from the slope ( $q_m$ ) and  
240 intercept ( $K_L$ ), and the model's characteristics can be expressed in terms of  $R_L$ , a dimensionless constant  
241 for the separation factor to depict whether the adsorption is favourable or unfavourable – Equation (6):

$$242 \quad R_L = \frac{1}{1+K_L C_i} \quad (6)$$

243 where,  $C_i$  is initial concentration. The characteristics of  $R_L$  for favourable adsorption are  $0 < R_L < 1$ , for  
244 unfavourable adsorption  $R_L > 1$ , for linear adsorption  $R_L = 1$ , and for irreversible adsorption  $R_L = 0$ .

### 245 **Reusability of nanofibers**

246 The reusability was determined by measuring the number of times an optimised weight of nanofiber  
247 could be used to lower dye concentration from a fresh solution to 50% of its initial value, each time. To  
248 do this the optimised weight of nanofiber was added to a 10 ml aliquot of 3 mg/L methylene blue  
249 solution at the optimised temperature and time. After treatment, the amount of dye remaining in solution  
250 was determined by colorimetry. Subsequently a fresh aliquot of dye solution was treated using the  
251 nanofibers from the previous test and the proportional dye removal calculated. The cycle was repeated  
252 until the proportional removal of dye was only 50%. In each cycle to evaluate reusability, the  
253 proportional desorption was also evaluated to gauge the nanofibers' uptake and thus determine their  
254 reusability. After adsorption the copolymer was re-dissolved in distilled water and the dye leaching  
255 from the polymer was studied to calculate desorption – Equation (7):

$$256 \quad \% \text{ desorption} = \frac{\text{Conc of dye leached}}{\text{Conc of dye adsorbed}} \times 100 \quad (7)$$

## 257 **Results and discussion**

### 258 **Determination of LCST of the copolymer**

259 The LCST values obtained from the CP measurements were confirmed using a differential scanning  
260 calorimeter. Figure 2a shows the thermogram for CoP-1 and Table 2 summarises the DSC events for

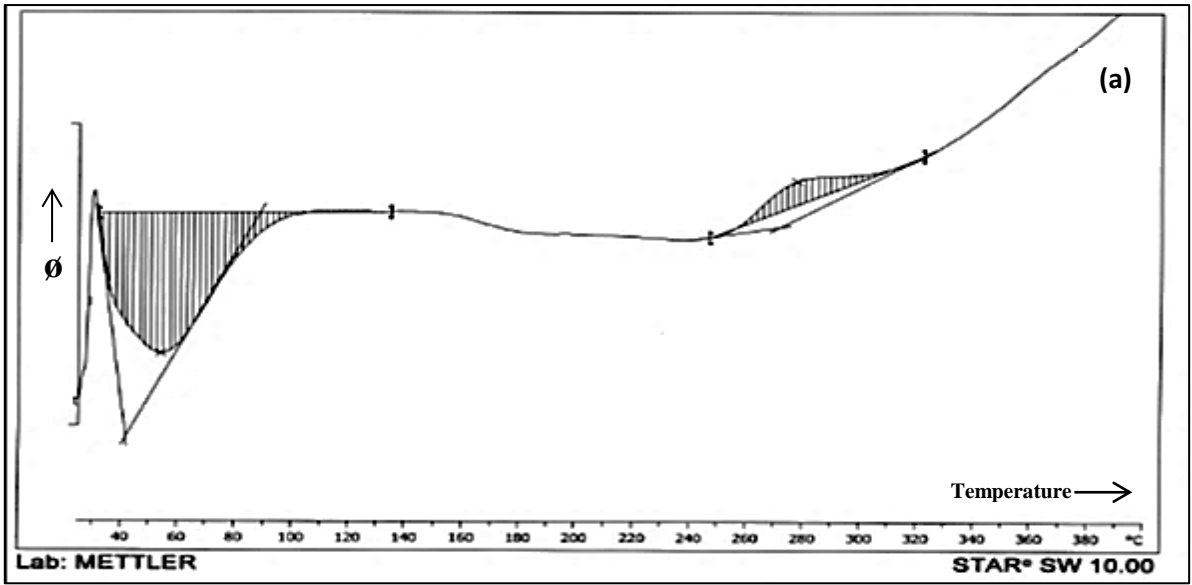
261 the other copolymers. The LCSTs of the homopolymers NIPAAM and DMAEMA are 32 and 49 °C  
262 respectively. It is noted that the LCST of the copolymers differs from those of the individual  
263 homopolymers, indicating that the LCST variation is due to increase/decrease of the hydrophilic  
264 properties of the copolymer owing to addition or change of functional groups.

#### 265 **FT-IR analysis**

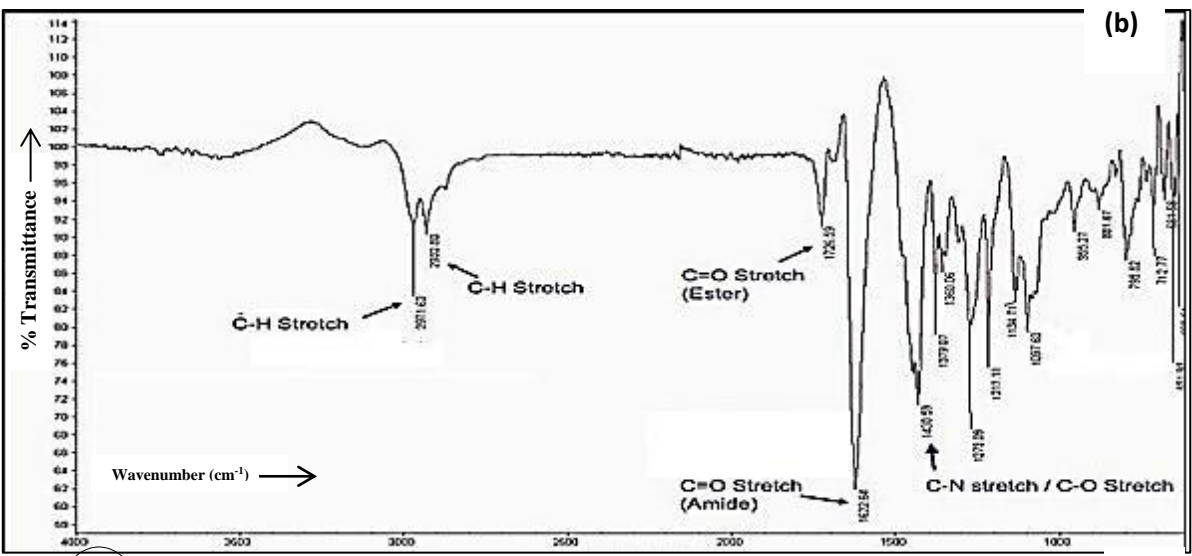
266 The FT-IR spectrum of copolymer CoP-1 confirms its structure as seen in Figure 2b. The absorption  
267 at 1726.5 cm<sup>-1</sup> is assigned to the ester C=O stretch, while the peak at 1622.84 cm<sup>-1</sup> is the amide group  
268 C=O. The presence of the ester and amide groups is reinforced by the absorption at 1430.6 cm<sup>-1</sup>, caused  
269 by the C-N and C-O stretches. The FT-IR spectra of the other copolymers reveal similar characteristics  
270 of successful copolymerization.

#### 271 **<sup>1</sup>H-NMR characterization**

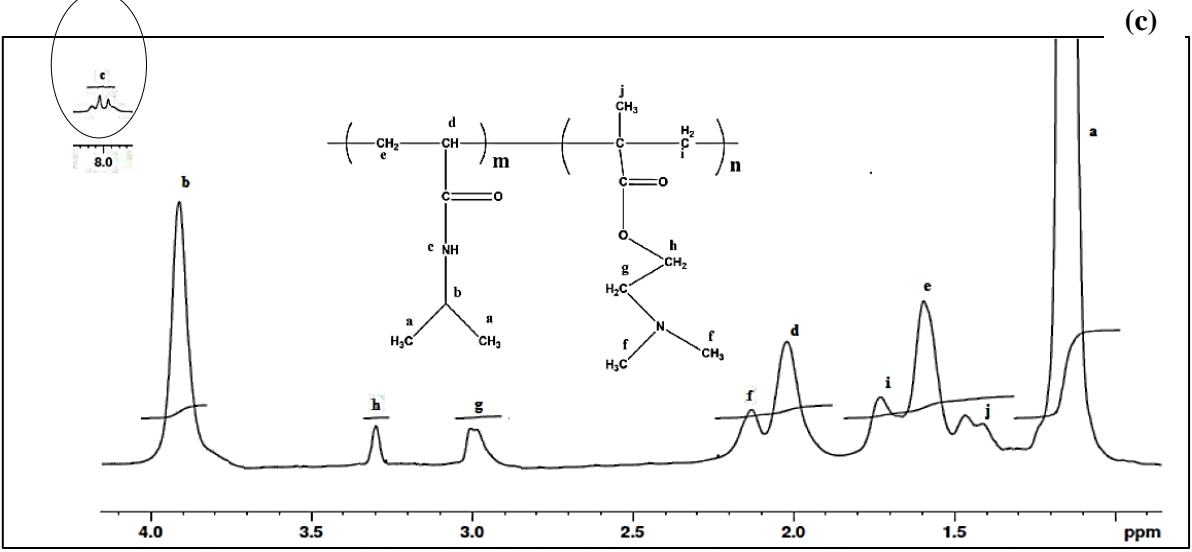
272 In the <sup>1</sup>H-NMR spectrum of CoP-1 (Figure 2c), the strong signal at 1.10 ppm is assigned to the -  
273 CH(CH<sub>3</sub>)<sub>2</sub> methyl from the isopropyl group in NIPAAM as is that at 3.90 ppm, while the resonance at  
274 2.10 ppm is the methyl resonance of the -N(CH<sub>3</sub>)<sub>2</sub> dimethyl group in DMAEMA.. The adjacent peaks  
275 at 3.00 and 3.30 ppm are from the (-N-CH<sub>2</sub>-CH<sub>2</sub>-O-) ethyl groups in DMAEMA. The signal at 1.60  
276 ppm is attributed to the methylene group (-CH<sub>2</sub>-CH-) from the NIPAAM backbone and that at 1.72 ppm  
277 is due to the methylene (-CH<sub>2</sub>-C-) from the DMAEMA backbone. The peak at 1.4 ppm is from the  
278 methyl group (CH<sub>3</sub>-C-) in DMAEMA. The resonance at 2.00 ppm is due to the methyne (-CH-CH<sub>2</sub>) in  
279 the NIPAAM backbone. The signal at 8.00 ppm is due to the (-NH-C=O) amide group in NIPAAM.  
280 The NMR spectrum thus confirms the presence of both NIPAAM and DMAEMA in the final  
281 copolymer. (The signal strengths show that NIPAAM is present in large excess over DMAEMA.)



282



283



284

285 **Figure 2. (a) DSC thermogram for CoP-1 (b) FT-IR spectrum of CoP-1 (c) <sup>1</sup>H-NMR spectrum**

286 **of CoP-1**



287 **Molecular weight determination**

288 **Gel permeation chromatography (GPC)**

289 The number average ( $M_n$ ), average molecular weight ( $M_w$ ) and dispersity (D) of the various  
290 thermoresponsive copolymers are given in Table 2. The uniform distribution of molecular weight in all  
291 three samples is confirmed because the D values are all close to unity.

---

Copolymer	Endothermic events ( $^{\circ}\text{C}$ )			Molecular weights		
	Onset (LCST)	Peak	Endset	$M_n$ (D)	$M_w$ (D)	D
CoP-1	37.5	62.5	86	71,460	71,893	1.01
CoP-2	25.6	39.5	53.7	25,171	31,091	1.23
CoP-4	44.2	65.1	90	30,026	32,490	1.08

---

292 **Table 2. Endothermic events by DSC and molecular weights by GPC for copolymers**

293 **Surface area and porosity**

294 The surface area and porosity of CoP-1 were calculated from the adsorption isotherm obtained by  
295 measuring the amount of gas adsorbed across a wide range of relative pressures from 10 to 70 Kpa at  
296 constant temperature (liquid nitrogen 77 K) in triplicate. The amount of gas adsorbed is correlated to  
297 the total surface area of the particles including pores in the surface. The BET specific surface of CoP-1  
298 was determined as 0.824  $\text{m}^2/\text{g}$ , while the BJH plot shows the pore specific surface as 0.901  $\text{m}^2/\text{g}$ .  
299 Although the copolymer has a relatively small surface area compared to conventional adsorbents – e.g.,  
300 activated charcoal (3,000  $\text{m}^2/\text{g}$ ) (Dillon Jr *et al.*, 1989) – it still exhibits effective adsorbent properties  
301 due to its high specificity at LCST, when the positions of the hydrophilic and hydrophobic groups are  
302 reversed in its regular structural scaffold. The presence of hydrophobic groups on the polymers'  
303 (adsorbate) surface results in low/no hydrogen bonding interaction with water molecules, thereby  
304 increasing the adsorbing surface, and thus the adsorption power and selectivity.

305 The BJH plot indicates pore volume and radius of 0.0073  $\text{cm}^3/\text{g}$  and 1.2 nm, respectively. The  
306 copolymer pore widths are between 2 and 10 nm, as observed in many adsorbents like zeolites. Thus

307 the copolymers can be classified as mesoporous according to the IUPAC classification (Dąbrowski,  
308 2001). The pore width of 2.4 nm of the copolymer CoP-1 suggests that the area available for adsorption  
309 is the same as for standard adsorbents.

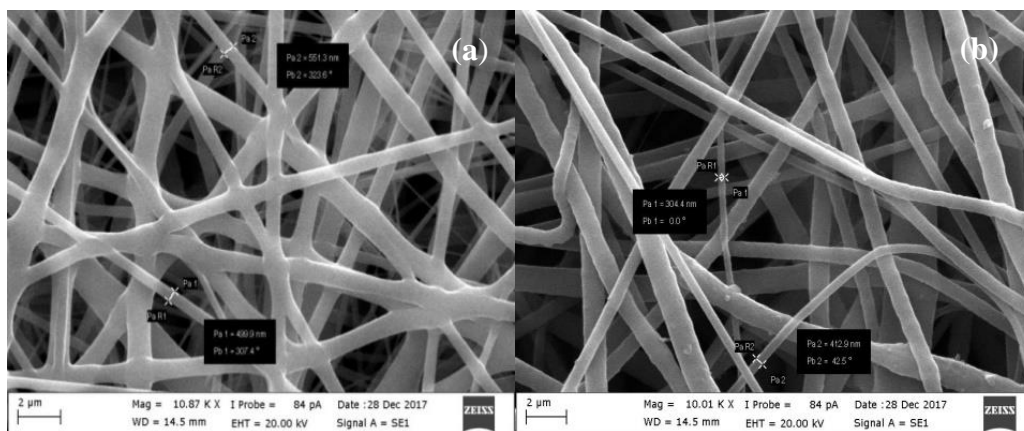
### 310 Copolymer particle size at CP

311 The particle size, measured when the polymer precipitates at the responsive temperature, is 606 nm,  
312 compared to 650 nm when measured at the responsive pH. Precipitation of the polymer as nanosize is  
313 largely responsible for the efficient dye adsorption above the CP.

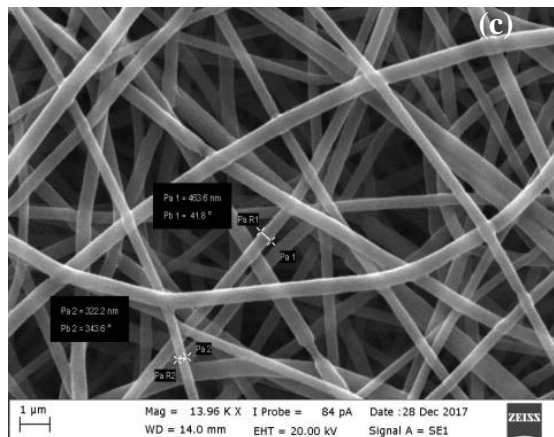
### 314 SEM analysis

315 Figure 3 shows SEM images of the nanofibers of two copolymers,. The nanofibers are seen to be  
316 distributed randomly in the composite. The diameter of the nanofibers was calculated from the SEM  
317 images. The average diameter (AFD), determined by measuring about one hundred fibers, is between  
318 300 and 500 nm, confirming the nanofiber structure.

319



320



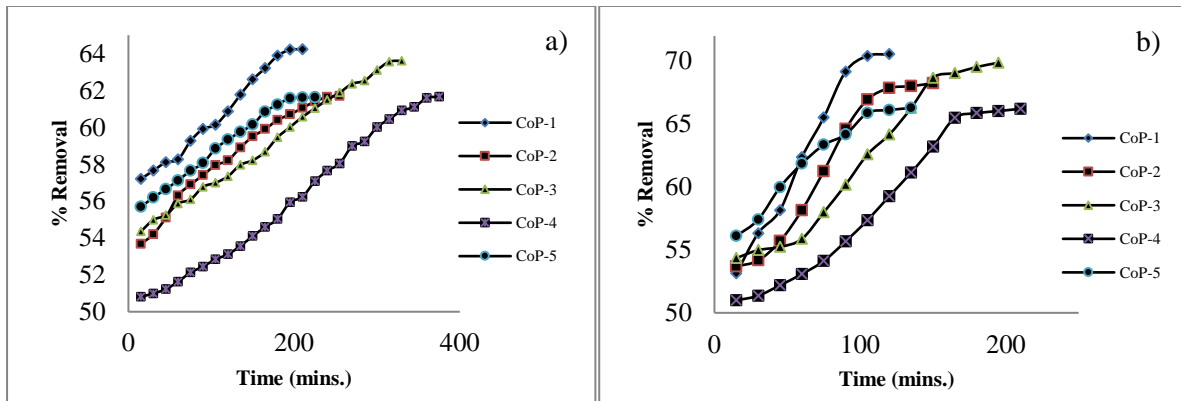
321

Figure 3. SEM images for (a) NF-1 (b) NF-2 (c) PCL

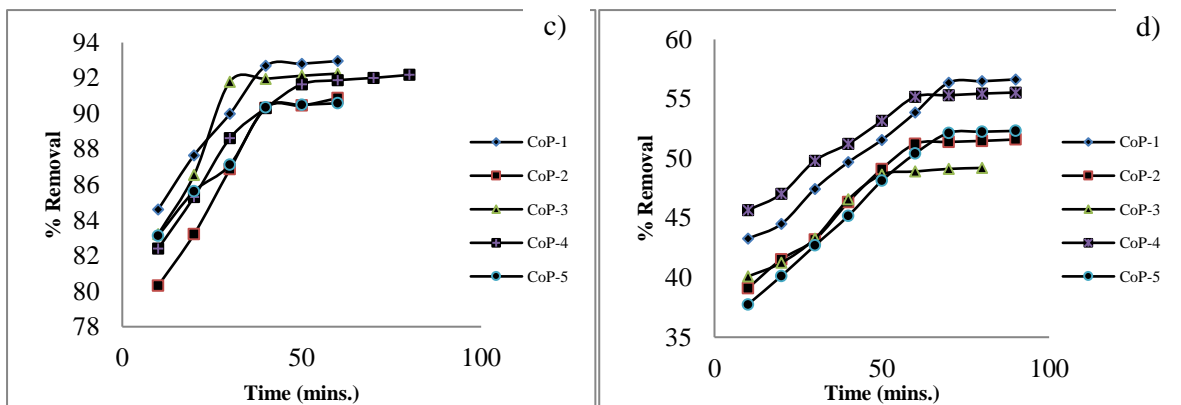
322 Adsorption parameter optimization

323 Dual responsive polymers extract dyes effectively at the defined concentrations as shown by the  
 324 decrease in absorbance with increasing contact time. Treatment continued until the solution reached  
 325 equilibrium; which was attained more rapidly as the polymer concentration was increased in solution  
 326 (Figure 4). The optimal copolymer concentrations and contact times were obtained for fixed dye  
 327 concentrations above the respective CPs (temperature and pH) at which adsorption was studied. The  
 328 optimised parameters for the copolymers treating a dye concentration of 3 mg/L are shown in Table 3.

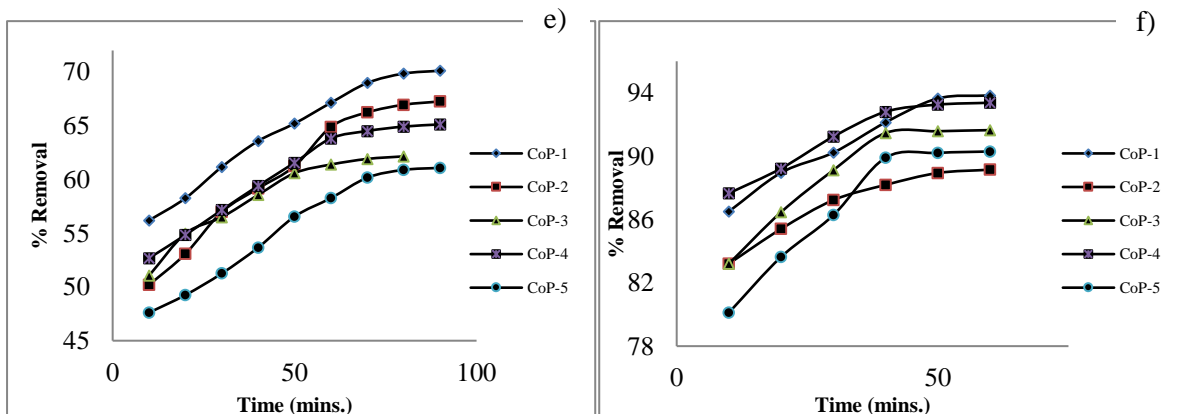
329



330



331



332 **Figure 4. Optimization of equilibrium contact time for maximum adsorption by various co-**  
333 **polymers at concentrations and responsive conditions as: (a) 1 mg/ml at LCST (b) 2 mg/ml at**  
334 **LCST (c) 4 mg/ml at LCST (d) 1 mg/ml at pH cloud point (e) 2 mg/ml at pH cloud point (f) 4**  
335 **mg/ml at pH cloud point. (Values are with mean $\pm$  s.d. of 0.95-1.66)**

336

337

338

339

<b>Proportional dye removal (methylene blue – 3 mg/mL) (%)</b>						
<b>Co-polymer (4 mg/ml)</b>	<b>Effect of temperature</b>			<b>Effect of pH</b>		
	proportional removal efficiency	Temperature	Equilibrium contact time (mins)	proportional removal efficiency	pH	Equilibrium contact time (mins)
<b>CoP-1</b>	92.77	40°C	40	93.84	10.5	30
<b>CoP-2</b>	90.15	35°C	40	88.26	10.5	50
<b>CoP-3</b>	91.32	35°C	50	90.17	12.5	40
<b>CoP-4</b>	92.11	50°C	60	93.38	11	40
<b>CoP-5</b>	90.49	55°C	40	89.91	10	50

**Table 3. Optimised conditions and maximum methylene blue removal efficiency by dual responsive polymers**

**Evaluation of adsorption potential under optimised conditions**

For a polymer concentration of 4 mg/ml, the optimal temperature, pH, contact times to clear a dye (e.g methylene blue at a concentration of 3 mg/L) was studied and the results are presented in Table 4. All of the dual responsive polymers tested exhibited similar extraction efficiencies for the various dyes. However, CoP-1 showed maximum dye removal in the shortest contact time under the respective temperature and pH CP conditions. Since both cationic and anionic dyes were tested, this suggests that extraction is independent of the dye’s charge and solely due to physical adsorption, extending the spectrum of applicability of the copolymers to a wide range of dyes.

**Evaluation of adsorption potential using nanofibers**

Studies were carried to determine the amount of nanofibers necessary to adsorb dye solutions of varying concentrations. This study established that 3 mg/ml nanofiber suspensions offer the maximum proportional adsorption of dye under the influence of respective trigger and contact time (Table 4). All three nanofibers – NF-1, NF-2 and NF-3 – showed slightly better dye adsorption efficiencies than the dual responsive copolymers (Table 3). PCL nanofibers also showed significant dye removal efficiency

356 and, as the copolymers are blended with PCL for nanofabrication, the combination tends to increase  
 357 their efficiency when converted to nanofibers.

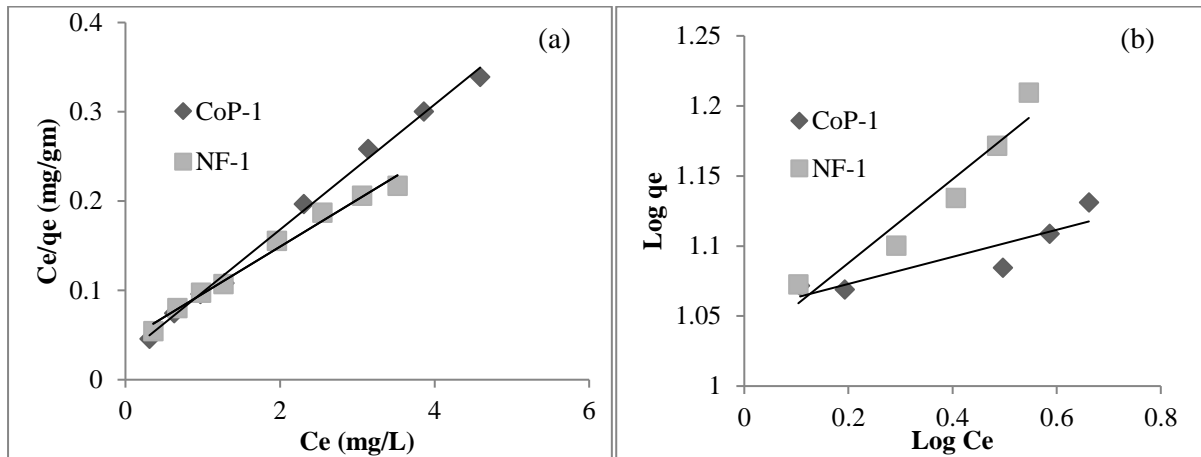
Adsorbent	Proportional dye removal (%)									
	Methylene blue (3 mg/L)		Methyl orange (3 mg/L)		Indigo carmine (12 mg/L)		Congo red (20 mg/L)		Crystal violet (6 mg/L)	
	Temp*	pH <sup>#</sup>	Temp*	pH <sup>#</sup>	Temp*	pH <sup>#</sup>	Temp*	pH <sup>#</sup>	Temp*	pH <sup>#</sup>
<b>CoP-1</b>	92.77	93.84	91.26	90.97	92.60	91.24	90.28	89.86	91.20	90.41
<b>CoP-2</b>	90.15	88.26	89.94	89.01	90.51	89.64	88.52	87.27	90.11	88.47
<b>CoP-3</b>	91.32	90.17	92.16	90.43	90.57	88.63	89.74	88.02	92.20	90.18
<b>CoP-4</b>	92.11	93.38	90.53	89.87	91.74	90.3	90.67	89.79	90.29	89.64
<b>CoP-5</b>	90.49	89.91	90.12	89.16	89.65	89.12	88.2	88.47	88.95	87.88
<b>NF-1</b>	99.01	96.21	98.12	94.98	98.52	97.13	96.85	95.24	97.59	96.48
<b>NF-2</b>	97.05	95.67	95.87	94.06	96.89	95.89	95.07	93.17	95.91	96.13
<b>NF-3</b>	97.89	96.19	95.03	94.17	96.71	94.89	94.18	92.54	93.95	94.37
<b>PCL</b>	54.51	53.24	49.12	51.36	53.96	51.79	56.32	55.14	50.26	49.85
<b>Blank</b>										

358 **Table 4. Proportional removal of dyes by dual responsive polymers (4 mg/ml) and nanofibers (3**  
 359 **mg/ml) under optimised conditions. [\*45°C, #12.0]**

360 **Adsorption isotherm analysis**

361 The CoP-1 and fiber NF-1 were studied using the Langmuir and Freundlich models. The models' terms  
 362 were calculated and R<sup>2</sup> values obtained for both isotherms (Figure 5). The value of R<sub>L</sub> shows that NF-1  
 363 adsorbs the dyes better than CoP-1; in other words, converting CoP-1 to the nanofiber form NF-1  
 364 increases dye adsorption efficiency.

365 Table 5 shows the constants for the two isotherm models and it is evident that the Langmuir model  
 366 provides a better fit than the Freundlich one for both CoP-1 ( $R^2 > 0.990$ ) and NF-1 ( $R^2 > 0.98$ ), indicating  
 367 monolayer adsorption on the adsorbent surfaces.



368

369 **Figure 5. Dye adsorption isotherm model onto copolymer and nanofiber substrates.**

370 **(a) Langmuir and (b) Freundlich.**

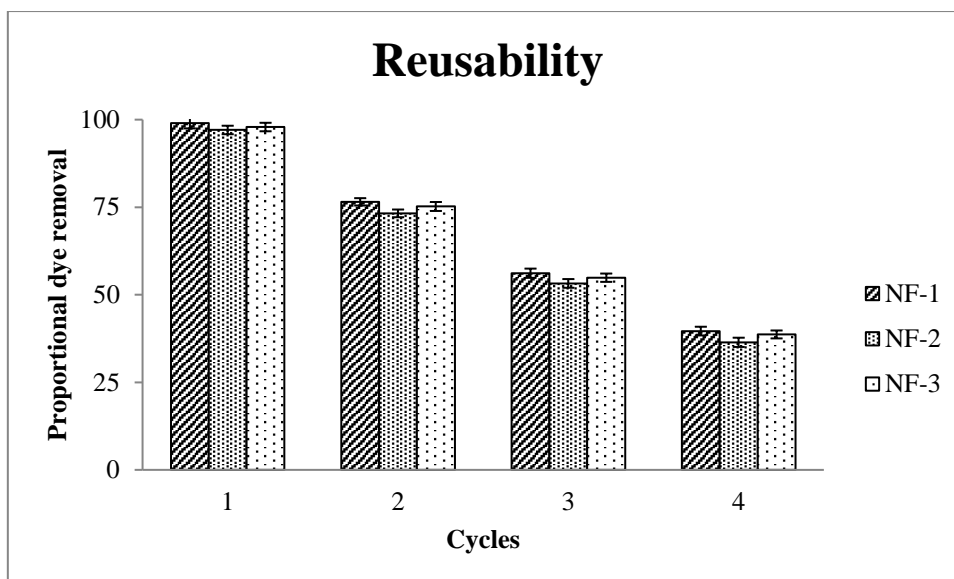
Adsorbent	Langmuir constants			Freundlich constants			
	$q_m$ (mg/g)	$K_L$ (L/mg)	$R^2$	$R_L$	$K_F$	$1/n$	$R^2$
CoP-1	14	3.078	0.9921	0.03	0.022	0.0965	0.8034
NF-1	19	1.20	0.9856	0.076	0.012	0.2987	0.9182

371 **Table 5. Langmuir and Freundlich isotherm constants for dye adsorption by CoP-1 and nanofiber**  
 372 **NF-1.**

373 **Nanofiber reusability**

374 This study was carried out at the optimised temperature, pH and time frame for maximum efficiency.  
 375 As shown in Figure 6, NF-1 has slightly better dye removal efficiency of the three nanofibers tested  
 376 when used repeatedly with fresh dye solution stock. All three nanofibers lose more than 50% of their  
 377 efficiency after 3 cycles of reuse.

378



379  
380 **Figure 6. Reusability of nanofibers**

381 **Conclusions**

382 The primary objective of the study was to develop dual responsive polymers that exhibit smart  
383 behaviour for dye removal from simulated textile water. The polymers used exhibited good adsorption  
384 efficiencies at various temperatures and pH levels. To improve the dye removal efficiency of the  
385 polymers, they were converted to nanofibers by electrospinning. Due to their high specific surface and  
386 sensitivity, nanofibers were found to be more effective for dye removal than polymer solutions.

387 **Acknowledgements**

388 The authors would like to thank (i) University Grants Commission (UGC), India [**File No.43/489 (SR)**]  
389 for providing financial assistance for this project. (ii) SLN pharmachem and ESS-EMM for the  
390 monomer gift samples. (iii) Kingston University, London for polymer sample analysis. (iv) Metrohm  
391 India PVT. LTD for the surface area and porosity determinations.

392 **References**

- 393 Aguliar M.R., Elvira C., Gallardo A., Vazquez B., Roman J.S. 2007 Smart polymers and their  
394 applications as biomaterials. *Topics in Tissue Engineering*, Vol. 3. Eds. Ashammakhi N, Reis R,  
395 Chiellini E
- 396 Akl, M.A., Abou-Elanwar, A.M. 2015 Adsorption studies of cd (II) from water by acid modified  
397 multiwalled carbon nanotubes. *Journal of Nanomedicine & Nanotechnology*, **6(6)**, 327-336.
- 398 Chen, L., Li, Y., Hu, S., Sun, J., Du, Q., Yang, X., Ji, Q., Wang, Z., Wang, D., Xia, Y. 2016 Removal  
399 of methylene blue from water by cellulose/graphene oxide fibress. *Journal of Experimental*  
400 *Nanoscience*, **11**, 1156-1170.



401 Dąbrowski, A. 2001 Adsorption—from theory to practice. *Advances in colloid and interface science*,  
402 **93**, 135-224.

403 Dillon Jr, E.C., Wilton, J.H., Barlow, J.C., Watson, W.A. 1989 Large surface area activated charcoal  
404 and the inhibition of aspirin absorption. *Annals of emergency medicine*, **18**, 547-552.

405 Elmoubarki, R., Mahjoubi, F., Tounsadi, H., Moustadraf, J., Abdennouri, M., Zouhri, A., El Albani, A.,  
406 Barka, N. 2015 Adsorption of textile dyes on raw and decanted Moroccan clays: Kinetics, equilibrium  
407 and thermodynamics. *Water Resources and Industry*, **9**, 16-29.

408 Hinrichs, W., Schuurmans-Nieuwenbroek, N., Van De Wetering, P., Hennink, W. 1999  
409 Thermosensitive polymers as carriers for DNA delivery. *Journal of controlled release*, **60**, 249-259.

410 Ismaya, E., Diantoro, M., Kusumaatmaja, A., Triyana, K. 2017 Preparation of PVA/TiO<sub>2</sub> Composites  
411 Nanofibers by using Electrospinning Method for Photocatalytic Degradation. *IOP Conference Series:  
412 Materials Science and Engineering*, **202**, 1-6.

413 Liang, C.-Z., Sun, S.-P., Li, F.-Y., Ong, Y.-K., Chung, T.-S. 2014 Treatment of highly concentrated  
414 wastewater containing multiple synthetic dyes by a combined process of coagulation/flocculation and  
415 nanofiltration. *Journal of Membrane Science*, **469**, 306-315.

416 Liang, M., Yang, T.-M., Chang, H.-P., Wang, Y.-M. 2015 Dual-responsive polymer–drug nanoparticles  
417 for drug delivery. *Reactive and Functional Polymers*, **86**, 27-36.

418 Marques, N.d.N., Maia, A.M.d.S., Balaban, R.d.C. 2015 Development of dual-sensitive smart polymers  
419 by grafting chitosan with poly (N-isopropylacrylamide): an overview. *Polímeros*, **25**, 237-246.

420 Paneyasar, J.S., Barton, S., Chandra, S., Ambre, P., Coutinho, E. 2017 Novel thermoresponsive  
421 assemblies of co-grafted natural and synthetic polymers for water purification. *Water Science and  
422 Technology*, **75** (5), 1084-1097.

423 Parasuraman, D., Serpe, M.J. 2011 Poly (N-isopropylacrylamide) microgels for organic dye removal  
424 from water. *ACS applied materials & interfaces*, **3**, 2732-2737.

425 Robinson, T., McMullan, G., Marchant, R., Nigam, P. 2001 Remediation of dyes in textile effluent: a  
426 critical review on current treatment technologies with a proposed alternative. *Bioresource technology*,  
427 **77**, 247-255.

428 Samah, N.H.A., Heard, C.M. 2013 Enhanced in vitro transdermal delivery of caffeine using a  
429 temperature- and pH-sensitive nanogel, poly (NIPAM-co-AAc). *International journal of pharmaceuticals*,  
430 **453**, 630-640.

431 Swaminathan, S., Muthumanickam, A., Imayathamizhan, N. 2015 An effective removal of methylene  
432 blue dye using polyacrylonitrile yarn waste/graphene oxide nanofibrous composite. *International  
433 journal of environmental science and technology*, **12**, 3499-3508.

434 Zheng, Y., Wang, L., Lu, L., Wang, Q., Benicewicz, B.C. 2017 pH and Thermal Dual-Responsive  
435 Nanoparticles for Controlled Drug Delivery with High Loading Content. *ACS Omega*, **2**, 3399-3405.

436 Zhu, C., Jung, S., Luo, S., Meng, F., Zhu, X., Park, T.G., Zhong, Z. 2010 Co-delivery of siRNA and  
437 paclitaxel into cancer cells by biodegradable cationic micelles based on PDMAEMA-PCL-  
438 PDMAEMA triblock copolymers. *Biomaterials*, **31**, 2408-2416.